Journal of Inorganic Biochemistry 195 (2019) 101–110

Contents lists available at ScienceDirect

Journal of Inorganic Biochemistry

journal homepage: www.elsevier.com/locate/jinorgbio

Zinc-oxaprozin compounds: Synthesis, structure and biological activity

Marialena Lazou[a], Antonios G. Hatzidimitriou[a], Athanasios N. Papadopoulos[b], George Psomas[a,*]

[a] Department of General and Inorganic Chemistry, Faculty of Chemistry, Aristotle University of Thessaloniki, GR-54124 Thessaloniki, Greece
[b] Department of Nutrition and Dietetics, Faculty of Food Technology and Nutrition, Alexandrion Technological Educational Institution, Sindos, Thessaloniki, Greece

ARTICLE INFO

Keywords:
Oxaprozin
Zinc complexes
Structures
Scavenging ability
DNA-binding
Interaction with albumins

ABSTRACT

Four novel zinc complexes, namely $[Zn(oxa)_2(MeOH)_4]$ (**1**), $[Zn(oxa)_2(H_2O)(bipy)]\cdot MeOH\cdot 2.5H_2O$ (**2**·MeOH·2.5H_2O), $[Zn(oxa)_2(bipyam)]\cdot 1.25MeOH$ (**3**·1.25MeOH) and $[Zn(oxa)_2(phen)]$ (**4**), with the non-steroidal anti-inflammatory drug oxaprozin (Hoxa) and a *N,N′*-donor heterocyclic ligand, such as 2,2′-bipyridylamine (bipyam), 1,10-phenanthroline (phen) or 2,2′-bipyridine (bipy), were characterized with physicochemical techniques, various spectroscopies and single-crystal X-ray crystallography. In these coordination compounds, the oxaprozin ligands are coordinated to zinc ion in a monodentate or a bidentate chelating binding mode. The antioxidant activity of the complexes was evaluated *via* their ability to scavenge *in vitro* 1,1-diphenyl-2-picrylhydrazyl, hydroxyl and 2,2′-azinobis-(3-ethylbenzothiazoline-6-sulfonic acid) radicals. The complexes bind to calf-thymus DNA *via* intercalation as suggested *via* a series of studies employing UV–vis spectroscopy, DNA-viscosity measurements and competition with ethidium bromide. The complexes may bind to serum albumins tightly and reversibly in order to get transferred through the bloodstream.

1. Introduction

Zinc is among the most abundant biometals in human body. It is used to regulate the metabolism of cells and is found in more than two hundred metalloenzymes [1,2]. Zinc oxide and other zinc compounds are applied as medicaments to treat skin infections and injuries, while the use of “Baby Zinc” in Asian and African countries has saved the lives of many children as it may treat infections causing uncontrollable diarrhea [3]. In addition, diverse zinc complexes have been reported in the literature for their potential antidiabetic [4], anti-inflammatory [5], antimicrobial [6], antioxidant [7], and anticancer [8] activity as well as the potential applications to the treatment of Alzheimer's disease [9]. Further, a lot of zinc complexes with non-steroidal anti-inflammatory drugs (NSAIDs) have been structurally characterized [10] including the NSAIDs aspirin [11], diclofenac [12], diflunisal [7], flufenamic acid [13–15], ibuprofen [16], indomethacin [17,18], mefenamic acid [19], naproxen [20], niflumic acid [21,22] and tolfenamic acid [23,24] as ligands. Most of the reported zinc-NSAID complexes, especially the mixed-ligand complexes with *N,N′*-donor co-ligands, have shown an enhanced biologic profile (DNA- and albumin-binding properties and antioxidant activity) in comparison to the corresponding free NSAID [10].

NSAIDs are the most frequently administrated analgesic, anti-inflammatory and antipyretic agents with known side-effects. Oxaprozin (Hoxa, Fig. 1(A)) is a phenylalkanoic acid NSAID with analgesic activity and is used to relieve pain associated with osteoarthritis and rheumatoid arthritis. Oxaprozin was found to be in significantly lower doses as active as aspirin showing milder gastrointestinal side-effects [25,26]. Moreover, it can also have a protective effect against the development of cancer or Alzheimer's disease [27]. Its poor aqueous solubility gives rise to formulation problems and limits its actual therapeutic effectiveness, causing variable bioavailability, and enhancing the appearance of adverse effects, such as in particular gastro-duodenal mucosal injury [27]. A thorough search in the literature has revealed only one structurally characterized dinuclear copper(II)-oxaprozinate complex of the formula $[Cu_2(oxa)_4(DMSO)_2]$ which has been also examined *in vitro* for its SOD-activity [28]. In this complex, the four oxaprozin ligands are deprotonated and are bound to copper(II) ions in a bidentate $\mu_{1,3}$-bridging mode leading to the formation of a paddle-wheel pattern between the two copper atoms [28].

As a continuation of our current project regarding metal-NSAID complexes [7,10,13,14,19,21,23,24], we present herein the preparation, the characterization and the biological activity (antioxidant activity, interaction with DNA and serum albumins) of the zinc complexes with the NSAID oxaprozin as ligand and the *N,N′*-donors 2,2′-bipyridine (bipy), 2,2′-bipyridylamine (bipyam) or 1,10-phenanthroline (phen) as co-ligands (Fig. 1(B)–(D)). The complexes $[Zn(oxa)_2(MeOH)_4]$ (**1**), $[Zn(oxa)_2(H_2O)(bipy)]\cdot MeOH\cdot 2.5H_2O$ (**2**·MeOH·2.5H_2O), $[Zn(oxa)_2(bipyam)]\cdot 1.25MeOH$

* Corresponding author.
E-mail address: gepsomas@chem.auth.gr (G. Psomas).

https://doi.org/10.1016/j.jinorgbio.2019.03.016
Received 12 February 2019; Received in revised form 12 March 2019; Accepted 18 March 2019
Available online 21 March 2019
0162-0134/ © 2019 Elsevier Inc. All rights reserved.

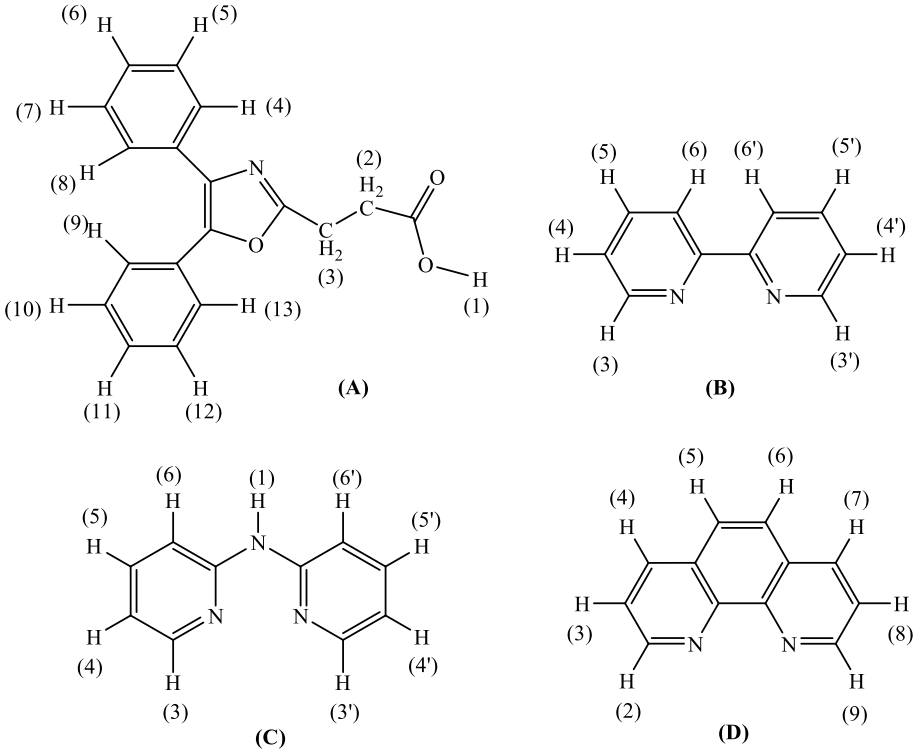

Fig. 1. The structural formula and hydrogen numbering of (A) oxaprozin (Hoxa), (B) 2,2′-bipyridine (bipy), (C) 2,2′-bipyridylamine (bipyam) and (D) 1,10-phenanthroline (phen).

(**3**·1.25MeOH) and [Zn(oxa)$_2$(phen)] (**4**) were isolated and characterized by diverse techniques such as elemental analysis, molar conductivity measurements, IR, UV–vis and ^{1}H NMR spectroscopies. The crystal structures of complexes **2–4** were determined by single-crystal X-ray crystallography. The complexes were also tested *in vitro* for their ability to scavenge free radicals such as 1,1-diphenyl-picrylhydrazyl (DPPH), hydroxyl (·OH) and 2,2′-azinobis-(3-ethylbenzothiazoline-6-sulfonic acid) (ABTS$^+$·). The ability of the complexes to bind to bovine (BSA) and human serum albumin (HSA) was investigated *in vitro* by fluorescence emission spectroscopy. The interaction mode and strength of complexes **1–4** with calf-thymus (CT) DNA was monitored directly by UV–vis spectroscopy, viscosity measurements and indirectly *via* their ability to displace the typical intercalator ethidium bromide (EB) from its conjugate with DNA (as explored by fluorescence emission spectroscopy).

2. Experimental

2.1. Materials and instrumentation

All chemical reagents used, *i.e.* oxaprozin, $ZnCl_2$, KOH, phen, bipy, bipyam, trisodium citrate, NaCl, CT DNA, EB, HSA, BSA, DPPH, ABTS, butylated hydroxytoluene (BHT), 6-hydroxy-2,5,7,8-tetramethylchromane-2-carboxylic acid (trolox) and nordihydroguaiaretic (NDGA) were purchased from Sigma-Aldrich and all solvents were purchased from Merck. All the chemicals and solvents were reagent grade and were used as purchased.

The DNA stock solution was prepared by dissolving CT DNA to a buffer solution (containing 150 mM NaCl and 15 mM trisodium citrate at pH 7.0) which was followed by 3-day stirring and was kept at 4 °C for no longer than two weeks. The concentration of this DNA solution was determined by the UV absorbance of a 1:20 diluted solution at 260 nm using $\varepsilon = 6600\ M^{-1}\,cm^{-1}$ [29]. The ratio of UV absorbance at 260 and 280 nm (A_{260}/A_{280}) of the stock DNA solution was in the range 1.85–1.90, which may imply the protein non-contamination of DNA [30].

Infrared (IR) spectra were recorded in the range 400–4000 cm^{-1}on a Nicolet FT-IR 6700 spectrometer with samples prepared as KBr pellets. UV–vis spectra were recorded in solution at concentrations in the range 10^{-5}–10^{-3} M on a Hitachi U-2001 dual beam spectrophotometer. C, H and N elemental analysis were performed on a PerkinElmer 240B elemental analyzer. ^{1}H NMR spectra were recorded at room temperature on an Agilent 500 NMR spectrometer using DMSO-d_6 as solvent. The molar conductivity measurements of a solution of the complexes in DMSO (1 mM) were performed with a Crison Basic 30 conductometer. The fluorescence spectra were recorded in solution on a Hitachi F-7000 fluorescence spectrophotometer. The viscosity experiments were performed with a Fungilab ALPHA L series rotational viscometer which was equipped with an 18-mL LCP spindle.

2.2. Synthesis of the complexes

2.2.1. Synthesis of [Zn(oxa)$_2$(MeOH)$_4$], 1

A methanolic solution (15 mL) containing oxaprozin (0.3 mmol, 88 mg) and KOH (0.3 mmol, 17 mg) was added, after 1-h stirring, dropwise to a methanolic solution (6 mL) of $ZnCl_2$ (0.15 mmol, 20 mg). The reaction solution was stirred for additional 30 min and was left to slowly evaporate. After ten days, colorless microcrystalline product of [Zn(oxa)$_2$(MeOH)$_4$] **1** (65 mg, 56%) was collected. *Anal.* calcd. for $C_{40}H_{44}N_2O_{10}Zn$ (MW = 778.17): C 61.74, 5.70, N 3.60; found C 61.55, 5.58, N 3.67%. IR (KBr disk), ν_{max}/cm^{-1}: $\nu_{asym}(CO_2)$: 1556 (*vs* (very strong)); $\nu_{sym}(CO_2)$: 1342 (strong (s)); $\Delta\nu(CO_2) = \nu_{asym}(CO_2) - \nu_{sym}(CO_2) = 214\ cm^{-1}$. UV–vis in DMSO, λ/nm ($\varepsilon/M^{-1}\,cm^{-1}$): 276 (14400). ^{1}H NMR in DMSO-d_6, δ/ppm: 2.61 (4H, t, H^2-oxa), 2.99 (4H, t, H^3-oxa), 7.41–7.32 (12H, d, H^5-, H^6-, H^7-, H^{10}-, H^{11}- and H^{12}-oxa), 7.54 (8H, d, H^4-, H^8-, H^9-, and H^{13}-oxa). The complex is soluble in DMF, $CHCl_3$ and DMSO. $\Lambda_M = 12\ S{\cdot}cm^2{\cdot}mol^{-1}$, 1 mM in DMSO.

2.2.2. Synthesis of [Zn(oxa)$_2$(H$_2$O)(bipy)]·MeOH·2.5H$_2$O, **2**·MeOH·2.5H$_2$O

A methanolic solution (10 mL) containing Hoxa (0.3 mmol, 88 mg) and KOH (0.3 mmol, 17 mg) was stirred for 1 h. Afterwards, this

solution was added dropwise and simultaneously with a methanolic solution (1 mL) of bipy (0.15 mmol, 23.4 mg) into a methanolic solution (6 mL) of $ZnCl_2$ (0.15 mmol, 20 mg). The resultant solution was stirred for 30 min and was left for slow evaporation. Colorless crystals of [Zn(oxa)$_2$(H$_2$O)(bipy)]·MeOH·2.5H$_2$O, **2**·MeOH·2.5H$_2$O, (70 mg, 52%) suitable for X-ray structure determination were collected after two weeks. *Anal.* calcd. for [Zn(oxa)$_2$(H$_2$O)(bipy)], $C_{46}H_{38}N_4O_7Zn$ (MW = 824.21): C 67.03, 4.65, N 6.80; found C 66.87, 4.57, N 6.72%. IR (KBr disk): ν_{max}/cm^{-1}: $\nu_{asym}(CO_2)$: 1600 (s); $\nu_{sym}(CO_2)$: 1374 (s); $\Delta\nu(CO_2) = 226\ cm^{-1}$; $\rho(C\text{-}H)_{bipy}$: 765(m (medium)). UV–vis in DMSO, λ/nm ($\varepsilon/M^{-1}\ cm^{-1}$): 280 (13600). ^{1}H NMR in DMSO-d_6, δ/ppm: 2.59 (4H, t, H^2– oxa), 2.97 (4H, t, H^3-oxa), 7.39–7.32 (12H, d, H^5-, H^6-, H^7-, H^{10}-, H^{11}- and H^{12}-oxa), 7.50 (8H, d, H^4-, H^8-, H^9- and H^{13}-oxa), 7.53 (2H, t, H^4 και H$^{4\prime}$-bipy), 8.00 (2H, t, H^5 και H$^{5\prime}$-bipy), 8.43 (2H, d, H^6 και H$^{6\prime}$-bipy), 8.70 (2H, d, H^3 και H$^{3\prime}$-bipy). The complex is soluble in DMSO, DMF and MeOH. $\Lambda_M = 7\ S{\cdot}cm^2{\cdot}mol^{-1}$, 1 mM in DMSO.

2.2.3. Synthesis of complexes 3 and 4

Complexes **3** and **4** were prepared in a similar way to complex **2** with the use of bipyam (0.15 mmol, 26 mg) for **3** and phen (0.15 mmol, 27 mg) for **4**, instead of bipy.

Colorless single-crystals of [Zn(oxa)$_2$(bipyam)]·1.25MeOH, **3**·1.25MeOH (105 mg, 81%) suitable for X-ray structure determination were collected after a week. *Anal.* calcd. for [Zn(oxa)$_2$(bipyam)] $C_{46}H_{37}N_5O_6Zn$ (MW = 821.21): C 67.28, 4.54, N 8.53; found C 67.06, 4.62, N 8.36%. IR (KBr disk): ν_{max}/cm^{-1}: $\nu_{asym}(CO_2)$: 1602, 1584 (s); $\nu_{sym}(CO_2)$: 1406, 1381 (s); $\Delta\nu(CO_2) = 221,\ 178\ cm^{-1}$; $\rho(C\text{-}H)_{bipyam}$: 775(m). UV–vis in DMSO, λ/nm ($\varepsilon/M^{-1}\ cm^{-1}$): 274 (13360). ^{1}H NMR in DMSO-d_6, δ/ppm: 2.62 (4H, t, H^2-oxa), 2.98 (4H, t, H^3-oxa), 6.90 (2H, t, H^4 and H$^{4\prime}$-bipyam), 7.41–7.32 (12H, d, H^5-, H^6-, H^7-, H^{10}-, H^{11}- and H^{12}-oxa), 7.41 (2H, m, H^6 and H$^{6\prime}$-bipyam), 7.48 (8H, d, H^4-, H^8-, H^9- and H^{13}-oxa), 7.52 (2H, t, H^5 and H$^{5\prime}$-bipyam), 7.72 (1H, s, H^1-bipyam),8.24 (2H, d, H^3 and H$^{3\prime}$-bipyam). The complex is soluble in DMSO. $\Lambda_M = 5\ S{\cdot}cm^2{\cdot}mol^{-1}$, 1 mM in DMSO.

Colorless crystals of [Zn(oxa)$_2$(phen)] **4** (75 mg, 60%) suitable for X-ray structure determination were collected after ten days. *Anal.* calcd. for [Zn(oxa)$_2$(phen)], $C_{48}H_{36}N_4O_6Zn$ (MW = 830.22): C 69.44, 4.37, N 6.75; found C 69.65, 4.53, N 6.87%. IR (KBr disk): ν_{max}/cm^{-1}: $\nu_{asym}(CO_2)$: 1594 (s); $\nu_{sym}(CO_2)$: 1404 (s); $\Delta\nu(CO_2) = 190\ cm^{-1}$; $\rho(C\text{-}H)_{phen}$: 730(m). UV–vis in DMSO, λ/nm ($\varepsilon/M^{-1}\ cm^{-1}$): 270 (18880). ^{1}H NMR in DMSO-d_6, δ/ppm: 2.55 (4H, t, H^2-oxa), 2.94 (4H, t, H^3-oxa), 7.35 (12H, d, H^5-, H^6-, H^7-, H^{10}-, H^{11}- and H^{12}-oxa), 7.46 (8H, d, H^4-, H^8-, H^9- and H^{13}-oxa), 7.87 (2H, m, H^3 and H^8-phen), 8.17 (2H, s, H^5 and H^6-phen), 8.75 (2H, d, H^4 and H^7-phen), 9.02 (2H, d, H^2 and H^9-phen). The complex is soluble in DMSO. $\Lambda_M = 13\ S{\cdot}cm^2{\cdot}mol^{-1}$, 1 mM in DMSO.

2.3. X-ray structure determination

Single-crystals of the studied samples **2–4** suitable for X-ray diffraction were mounted on a Bruker Kappa APEX 2 diffractometer, equipped with a triumph monochromator using MoKa radiation at ambient temperature. Cell dimensions refinement was accomplished using at least 100 high θ reflections. The crystal presented no decay during the data collection. The frames collected (running φ and ω scans) were integrated with the Bruker SAINT Software package [31], using a narrow-frame algorithm. Data were corrected using the SADABS program [32]. The structures were solved by the SUPERFLIP package [33]. Crystals program package version 14.61 [34] has been used for the refinement and all the rest subsequent calculations through full-matrix least-squares on F^2. All non-hydrogen non disordered atoms have been refined anisotropically. For the disordered solvent atoms, their occupation factors were first refined under fixed isotropic factors values of 0.05 and finally their isotropic factors were refined under fix occupation using suitable geometry restraints. Hydrogen atoms bonded to non-disordered atoms were found at their expected positions and refined using proper riding constraints to the pivot atoms. CAMERON program has been used to produce molecular illustrations [35]. Crystallographic and experimental details are summarized in Table S1.

2.4. Biological activity studies

Due to low solubility of complexes **1–4** in water, the compounds were initially dissolved in DMSO (1 mM) during the experiments to study *in vitro* their biological activity, *i.e.* free radical scavenging, interaction with DNA or albumins. Mixing of such solutions with the aqueous buffer solutions of DNA or albumins used in the studies never exceeded 5% DMSO (*v*/v) in the final solution.

The antioxidant activity of Hoxa and its zinc complexes **1–4** was evaluated *via* their ability to scavenge *in vitro* DPPH, hydroxyl and ABTS radicals. The BSA- or HSA-binding studies were performed by tryptophan fluorescence quenching experiments. The interaction of the compounds with CT DNA was studied by UV–vis spectroscopy and viscosity measurements and *via* competitive studies with EB by fluorescence emission spectroscopy. Detailed procedures regarding the study of the biological activity of the compounds are given in the Supporting Information.

3. Results and discussion

3.1. Synthetic considerations

The synthesis of the complexes in high yield was achieved *via* the aerobic reaction of a basic solution of oxaprozin with a methanolic solution of $ZnCl_2$ (in a 1:2 Zn^{2+}:oxa^{-1} ratio) in the absence or presence of the corresponding *N,N′*-donor co-ligand (phen, bipyam or bipy). The absence of any *N,N′*-donor ligand led to the formation of complex **1**, while complexes **2–4** resulted from a 1:2:1 Zn^{2+}:oxa^{-1}:*N,N′*-donor reaction ratio. The characterization of the complexes was performed by IR, UV–vis and ^{1}H NMR spectroscopies, elemental analysis, molar conductivity measurements and single-crystal X-ray crystallography.

According to the results of elemental analysis, complex **1** has a 1:2 Zn:oxa composition and complexes **2–4** possess a 1:2:1 Zn:oxa:N,N′-donor composition. Compounds **1–4** are air-stable, soluble mainly in DMSO and insoluble in most common organic solvents and water. The molar conductivity values (Λ_M = 5–13 $S{\cdot}cm^2{\cdot}mol^{-1}$ for 1 mM DMSO solution) indicate the non-electrolytic nature of the complexes in DMSO solution (in the case of a 1:1 electrolyte, the Λ_M value of a 1 mM DMSO solution should be higher than 70 $S{\cdot}cm^2{\cdot}mol^{-1}$ [36]) and may suggest, thus, their integrity in solution.

3.2. Spectroscopic characterization of the complexes

Complexes **1–4** have been characterized by IR, ^{1}H NMR and UV–vis spectroscopies.

The deprotonation of oxaprozin, its binding mode to zinc and the existence of the N,N′-donors as co-ligands in complexes **2–4** was studied by IR spectroscopy [37]. The absorption band at 3424(broad, m) cm^{-1} in the IR spectrum of Hoxa which was attributed to the ν(O—H) stretching vibration of the carboxylic group of free Hoxa disappeared in the IR spectra of the complexes, revealing, thus, the deprotonation of oxaprozin. The bands located at 1720(s) cm^{-1} and 1274(s) cm^{-1} assigned to the $\nu(C{=}O)_{carboxylic}$ and $\nu(C{-}O)_{carboxylic}$ stretching vibrations, respectively, of the carboxylic group (—COOH) of free oxaprozin shifted in the IR spectra of complexes **1–4**. These bands appeared in the range of 1556–1602 cm^{-1} and 1342–1406 cm^{-1} and may be assigned to antisymmetric [$\nu_{asym}(CO_2)$] and symmetric [$\nu_{sym}(CO_2)$] stretching vibrations of the carboxylato group, respectively. For complexes **1**, **2** and **4**, the parameter $\Delta\nu(CO_2)$ ($=\nu_{asym}(CO_2)\text{-}\nu_{sym}(CO_2)$) bears values in the range 190–226 cm^{-1}, suggesting a monodentate binding fashion of the carboxylato group of oxaprozin ligand [37]. For complex **3**, two $\Delta\nu(CO_2)$ values were calculated ($=$178 and 221 cm^{-1}), suggesting that

the carboxylato ligands may exist in two different binding modes. All these results concerning the $\Delta\nu(CO_2)$ values are in good agreement with the structures of the complexes as they were determined by single-crystal X-ray crystallography and are discussed in section 3.3. Furthermore, in the IR spectra of complexes **2–4**, characteristic bands of the out-of plane ρ(C−H) vibrations of the corresponding *N,N′*-donor were assigned; *i.e.* for $\rho(C\text{-}H)_{bipy}$ in **2** at 765(m) cm^{-1}, for $\rho(C\text{-}H)_{bipyam}$ in **3** at 775(m) cm^{-1}, and for $\rho(C\text{-}H)_{phen}$ in **4** at 730(m) cm^{-1}. The presence of these discrete bands verifies the existence of the corresponding *N,N′*-donor as co-ligands in the complexes and their coordination [37].

The ^1H NMR spectra of complexes **1–4** were recorded in DMSO-d_6 solution in order to examine the behavior of the complexes in solution. In the ^1H NMR spectra of the complexes (Fig. S1), the signals attributed to the aromatic hydrogen atoms of oxaprozin ligands are slightly shifted upfield or downfield as expected upon their binding to Zn(II) ion. Furthermore, the signals expected for the H atoms of the *N,N′*-donor co-ligands have been also assigned in the ^1H NMR spectra of complexes **2–4** and, after integration of peaks, the ratio of the ligands (oxa:*N,N′*-donor) in the solid state has been also confirmed [21,23,24]. The absence of any other signals attributable to dissociated ligands may indicate the integrity of the complexes in solution, a fact being in accordance to the molar conductance measurements.

The UV–vis spectra of the complexes were recorded in DMSO solution and in the presence of buffer solution (150 mM NaCl and 15 mM trisodium citrate, pH = 7) used in the biological studies. All the recorded spectra exhibit similar pattern verifying that the complexes keep their integrity in these solution. Therefore, from all these studies concerning the solution behavior of the complexes (no new species in the ^1H NMR spectra are observed, complexes **1–4** do not dissociate in DMSO and present similar UV–vis spectral patterns in diverse solution mixtures), we may conclude that the complexes are stable in solution and keep their structural integrity.

3.3. Structure of the complexes

3.3.1. Crystal structure of complex *2*

The compound crystallizes in monoclinic system and space group $P2_1/c$ and there are two $[Zn(oxa)_2(H_2O)(bipy)]$ molecules, two badly disordered methanol and five water solvate molecules in the unit cell. The molecular structure of complex $[Zn(oxa)_2(H_2O)(bipy)]$ **2** is depicted in Fig. 2, and selected bond distances and angles are cited in Table 1.

In the mononuclear complex **2**, the oxaprozin ligands are deprotonated and are coordinated to zinc atom in a monodentate fashion *via* a carboxylate oxygen. The five-coordinate zinc atom is surrounded by oxygen atoms O(1) and O(4) from two monodentate oxaprozin ligands, two nitrogen atoms N(1) and N(2) from the bidentate bipy ligand and an oxygen atom O(7) from the aqua ligand. The trigonality index τ_5 ($\tau_5 = (\alpha-\beta)/60°$, where α and β (α > β) are the largest angles in the coordination sphere; $\tau_5 = 0$ is characteristic of a perfect square pyramid, and $\tau_5 = 1$ of a perfect trigonal bipyramid [38]) is equal to $(162.62° - 132.31°)/60° = 0.505$; this value of τ_5 may reveal that Zn(1) possesses an intermediate geometry between square pyramidal and trigonal bipyramidal. The distances around Zn(1) are within the expected range but are quite different; the Zn(1)−O bond distances (=1.952(2) – 2.072(2) Å) are shorter than the Zn(1)-N distances (=2.116(3) – 2.158(3) Å).

The solvate methanol and water molecules are H-bonded with the molecule resulting in a stabilized structure. The oxygen atoms O(1), O(2) and O(5) from the carboxylato groups as well as the nitrogen atoms N(3) and N(4) are interacting with the solvate water and methanol molecules from the title and neighboring symmetrically generated molecules forming a strong net. The coordinated O(7) from the aqua ligand is also interacting inter- and intra-molecular with O(5) (carboxylato) and O(8) (solvate water) completing the hydrogen-bonding net formation for further more structure stabilization. Hydrogen-bonding interactions are summarized in Table S2.

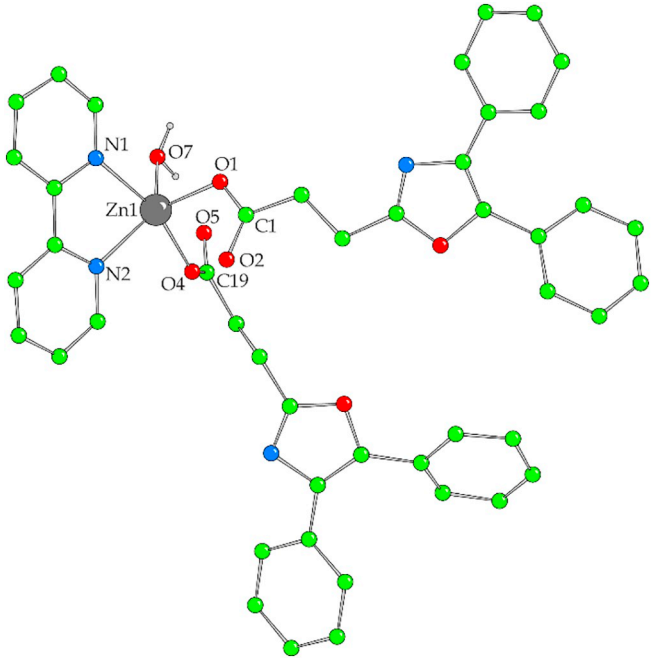

Fig. 2. The molecular structure of complex **2**.

Table 1
Selected bond distances (Å) and angles (°) in complex **2**.

Bond	Distance (Å)	Bond	Distance (Å)
Zn(1)−O(1)	1.952(2)	O(1)−C(1)	1.251(4)
Zn(1)−O(4)	2.072(2)	O(2)−C(1)	1.251(4)
Zn(1)−O(7)	2.072(2)	O(4)−C(19)	1.230(4)
Zn(1)−N(1)	2.158(3)	O(5)−C(19)	1.251(5)
Zn(1)−N(2)	2.116(3)		

Bonds	Angle (°)	Bonds	Angle (°)
O(1)−Zn(1)−O(4)	99.92(10)	O(4)−Zn(1)−O(7)	91.90(10)
O(1)−Zn(1)−O(7)	98.01(11)	O(4)−Zn(1)−N(1)	162.62(10)
O(1)−Zn(1)−N(1)	97.05(11)	O(4)−Zn(1)−N(2)	89.34(11)
O(1)−Zn(1)−N(2)	128.66(11)	O(7)−Zn(1)−N(1)	89.41(10)
N(1)−Zn(1)−N(2)	77.07(10)	O(7)−Zn(1)−N(2)	132.31(10)

3.3.2. Crystal structure of complex *3*

The molecular structure of complex $[Zn(oxa)_2(bipyam)]$, **3**, is shown in Fig. 3 and selected bond distances and angles are listed in Table 2.

In the mononuclear complex **3**, the two deprotonated oxaprozin ligands are coordinated to Zn atom in two different binding fashions: one oxaprozin ligand is bound to zinc ion monodentately *via* a carboxylate oxygen atom (*i.e.* O(4)), while the second oxaprozin ligand is bound to zinc in a bidentate chelating mode *via* atoms O(1) and O(2). Similar differentiation of coordination mode of the two NSAID ligands (*i.e.* one monodentate and one chelating bidentate NSAID ligand) is not the usual case and it has been previously found in few examples, *i.e.* the structures of six-coordinate complexes [Zn(mefenamato-O)(mefenamato-O,O′)(phen)(H_2O)] [19], [Mn(tolfenamato-O)(tolfenamato-O,O′)(phen)(H_2O)] [39], [Ni(naproxen-O)(naproxen-O,O′)(bipy)(MeOH)] and [Ni(naproxen-O)(naproxen-O,O′)(phen)(H_2O)] [40], [Mn(naproxen-O)(naproxen-O,O′)(phen)(H_2O)] [41] and the five-coordinate [Zn(niflumato-O)(niflumato-O,O′)(bipyam)] [21].

The bipyam ligand is bound to Zn *via* nitrogen atoms N(1) and N(2)

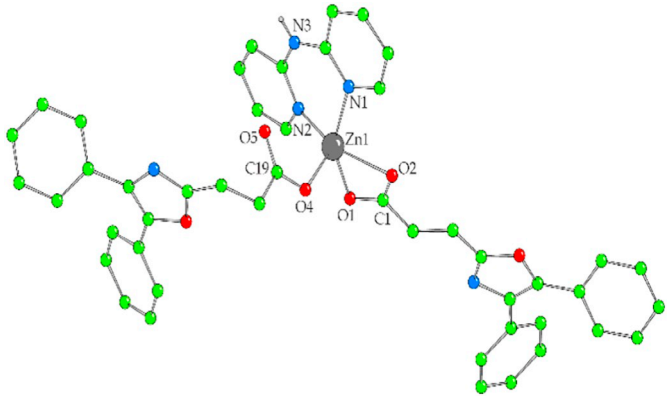

Fig. 3. The molecular structure of complex **3**.

Table 2
Selected bond distances (Å) and angles (°) in complex **3**.

Bond	Distance (Å)	Bond	Distance (Å)
Zn(1)–O(1)	2.129(3)	O(1)–C(1)	1.237(5)
Zn(1)–O(2)	2.185(3)	O(2)–C(1)	1.235(6)
Zn(1)–O(4)	1.980(3)	O(4)–C(19)	1.274(4)
Zn(1)–N(1)	2.031(3)	O(5)–C(19)	1.231(5)
Zn(1)–N(2)	2.029(3)		

Bonds	Angle (°)	Bonds	Angle (°)
O(1)–Zn(1)–O(2)	59.82(12)	O(2)–Zn(1)–O(4)	101.83(14)
O(1)–Zn(1)–O(4)	97.67(11)	O(2)–Zn(1)–N(1)	93.44(13)
O(1)–Zn(1)–N(1)	146.11(12)	O(2)–Zn(1)–N(2)	138.03(14)
O(1)–Zn(1)–N(2)	95.62(12)	O(4)–Zn(1)–N(1)	108.74(13)
N(1)–Zn(1)–N(2)	91.75(13)	O(4)–Zn(1)–N(2)	115.70(12)

which form a six-membered chelate ring. The geometry around the five-coordinate zinc atom is a slightly distorted square pyramid. In complex **3**, the trigonality index τ_5 has a value of 0.134 (=(146.11° – 138.03°) / 60°) which indicates slight distortion from the regular square-based pyramidal geometry [38]. The nitrogen atoms N(1) and N(2) of the bipyam ligand and the oxygen atoms O(1) and O(2) of the chelating oxaprozin ligand form the basal plane of the pyramid, while O(4) of the monodentate oxaprozin ligand lies at the apical position. The distances around Zn(1) are quite different with the Zn(1)–O(4) bond distance (=1.980(3) Å) being the shortest one, while the Zn(1)–$O_{(chelating)}$ bond distances are much longer (Zn(1)–O(1) = 2.129(3) Å and Zn(1)–O(2) = 2.185(3) Å).

The solvate methanol molecule is H-bonded with the coordinated oxygen O(4) (H(71)…O(4) = 1.95 Å, O(7)…O(4) = 2.775(8) Å, O(7)–H(71) = 0.83 Å and O(7)–H(71)…O(4) = 171°). An intermolecular H-bond between the imine hydrogen H(474) of the bipyam ligand and the non-coordinated O(5)′ of an adjacent molecule (H(474)…O(5)′ = 1.94 Å, N(3)…O(5)′ = 2.790(8) Å, N(3)–H(474) = 0.85 Å and N(3)–H(474)…O(5)′ = 176°) results in further stabilization of the structure.

3.3.3. Crystal structure of complex *4*

The molecular structure of complex [Zn(oxa)$_2$(phen)], **4** is shown in Fig. 4 and selected bond distances and angles are listed in Table 3.

In the mononuclear complex **4**, the two deprotonated oxaprozin ligands are bound to zinc ion monodentately *via* a carboxylate oxygen atom (O(1), O(1)′). The four-coordinate zinc atom is surrounded by two oxaprozin ligands and a bidentate phen ligand and possesses a slightly distorted tetrahedral geometry. The tetrahedrality for a four-coordinate metal atom can be determined from the angle subtended by two planes, each encompassing the metal and two adjacent atoms [42]; for strictly square planar complexes with D_{4h} symmetry, the tetrahedrality is 0°; for tetrahedral complexes with D_{2d} symmetry, the tetrahedrality equals 90°). For complex **4**, the dihedral angle between the planes formed by Zn(1), O(1) and N(1) (plane 1) and Zn(1), O(1)′ and N(1)′ (plane 2) is 76.95°, supporting the tetrahedral arrangement of the atoms around Zn (1).

The tetrahedral geometry around Zn(1) was further verified by the values of tetrahedral index τ_4 or τ'_4 as introduced by Yang [43] and Okuniewski [44], respectively. The values of these parameters are $\tau_4 = 0.81$ ($\tau_4 = (360° - (\alpha + \beta)) / (360° - 2 \times 109.5°)$, where α and β are the largest angles around the metal [43]) and $\tau'_4 = 0.72$ ($\tau'_4 = ((\beta-\alpha) / (360° - 109.5°)) + ((180° - \beta) / (180° - 109.5°))$ where β > α are the largest angles of the coordination sphere [44]) and are close to 1 supporting a tetrahedral geometry around Zn(1).

The Zn(1)–O bond distances (=1.945(2) Å) are shorter than the Zn (1)-N bond distances (=2.091(3) Å) and are within the expected range. The non-coordinated oxygen atoms of the oxaprozin ligands, O(2) and O(2)′, are 2.573(2) Å away from Zn(1) and are lying at the borderline of bonding interaction distances for Zn providing, thus, a distorted pseudo-octahedral geometry around Zn, if they were assumed as bonding distances.

Unlike complexes **2** and **3**, there are not any H-bonds observed in the structure of the complex. The asymmetric unit comprises half the molecule. The second half is symmetrically generated as to the C_2 axis passing through the metal ion and the mid distance between N(1) and N (1)′. The two individual molecules in the unit cell are arranged with the phenanthroline ligands being almost planar and lying on a0b crystallographic plane together with the Zn cation.

3.3.4. Proposed structure for complex [Zn(oxa)$_2$(MeOH)$_4$], *1*

Based on the IR and ^{1}H NMR spectra, and the results of elemental analysis data and molar conductivity, complex **1** is stable in solution with the same structure as in solid-state. On the basis of the elemental analysis and molar conductivity data, complex **1** is a neutral mononuclear complex. According to IR spectral data, the deprotonated oxaprozin ligands are coordinated to zinc ion in a monodentate manner *via* carboxylato oxygen atoms. As a conclusion, the zinc atom is six-coordinate bearing a ZnO_6 coordination sphere with a distorted octahedral geometry where four oxygen atoms from the methanol ligands and two oxygen atoms from the oxaprozin ligands occupy the vertices of the octahedron. Complex **1** is expected to have similar arrangement of the ligands around Zn with that reported for [Zn(niflumato-O)$_2$(MeOH)$_4$] [21].

3.4. Radical scavenging activity of the compounds

Free radicals are species responsible for the inflammations [45]; compounds that can scavenge free radicals or inhibit their production may be a useful tool in the treatment of inflammations. Since oxaprozin is used as an anti-inflammatory agent, we have investigated *in vitro* the ability of oxaprozin and its Zn(II) complexes **1–4** to scavenge DPPH, ABTS and hydroxyl radicals. The scavenging activity of complexes **1–4** has been also compared with that of the well-known antioxidant agents NDGA, BHT and trolox, which are the most commonly used standard reference antioxidant agents [46–48], and the results are summarized in Table 4.

The DPPH-scavenging ability of compounds has been often related to their potential antiageing, anticancer and anti-inflammatory activity [49]. The DPPH-scavenging ability of Hoxa and complexes **1–3** was found time-independent, while for complex **4** the DPPH-scavenging activity increased about ~11.5% upon time. In addition, the complexes were much more active than free Hoxa and reference compound BHT and some of them are slightly less active than the second reference compound NDGA. Complexes **1–4** present the best DPPH-scavenging activity among the reported metal-NSAID complexes [7,10,14,19,21,23,39–41,50–53]. Complex [Zn(oxa)$_2$(H_2O)(bipy)] **2** shows the highest DPPH-scavenging activity among the complexes.

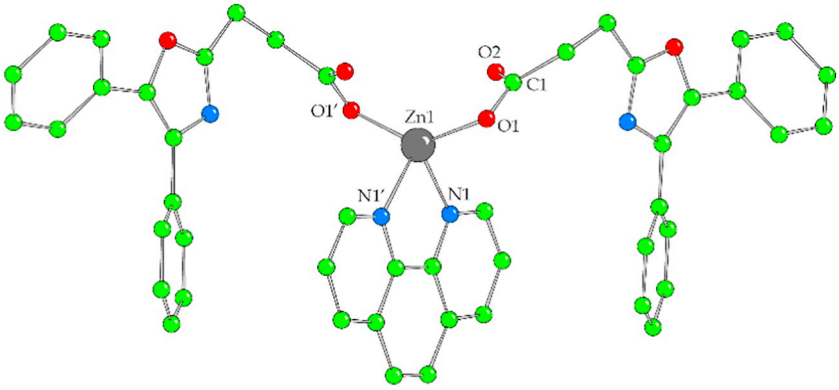

Fig. 4. The molecular structure of complex **4**.

Table 3
Selected bond distances (Å) and angles (°) in complex **4**.

Bond	Distance (Å)	Bond	Distance (Å)
Zn(1)−O(1)	1.945(2)	O(1)−C(1)	1.279(3)
Zn(1)−N(1)	2.091(3)	O(2)−C(1)	1.231(3)

Bonds	Angle (°)	Bonds	Angle (°)
O(1)−Zn(1)−O(1)′	138.26(13)	O(1)′−Zn(1)−N(1)	107.14(10)
O(1)−Zn(1)−N(1)	104.45(9)	O(1)′−Zn(1)−N(1)′	104.45(9)
O(1)−Zn(1)−N(1)′	107.14(10)	N(1)−Zn(1)−N(1)′	80.38(18)

Symmetry code: (′) $-x+1, y, -z+2$.

The scavenging of hydroxyl radicals has been mostly exhibited by compounds which may provide relief from the effects of reactive oxygen species [49]. According to our findings (Table 4), the complexes exhibit relatively high scavenging ability towards hydroxyl radicals. The hydroxyl scavenging ability of complexes **1–4** is better than that of free Hoxa and close to that of the reference compound trolox; in particular, complex [Zn(oxa)$_2$(H$_2$O)(bipy)] **2** is even more potent hydroxyl-scavenger than trolox.

The ability to scavenge the cationic ABTS radicals (ABTS$^+$·) has often served as a marker of the total antioxidant activity [49]. Complexes **1–4** are more active ABTS scavengers than free Hoxa but significantly less active than the reference compound trolox. Complex [Zn(oxa)$_2$(bipyam)] **3** is the best ABTS-scavenger among the compounds under study.

In general, the Zn-oxaprozin complexes **1–4** are better radical scavengers than free oxaprozin indicating that enhanced scavenging activity towards DPPH, hydroxyl and ABTS radicals may result from its coordination to Zn(II). In comparison with the existing metal-NSAID analogues [7,10,14,19,21,23,39–41,50–53], the present Zn-oxaprozin complexes **1–4** are significantly active DPPH- and hydroxyl-scavengers and moderate ABTS-scavengers.

3.5. Interaction of the compounds with albumins

Serum albumins (SAs) are the most abundant serum proteins, being responsible to transport drugs and metal ions to their biological targets, *i.e.* cells and tissues [54]. Within this context, studying the interaction of SA with candidate bioactive compounds (*e.g.* reported complexes **1–4**) may be a first approach to further explore the biological activity, since the biological properties of the compounds may differentiate upon binding to SA and/or novel transportation pathways or action mechanisms may be found [55].

The interaction of the compounds with both albumins, *i.e.* HSA and its homologue BSA, was monitored by fluorescence emission spectroscopy. The excitation of the buffer solutions of HSA and BSA at 295 nm results in the appearance of an intense emission band at $\lambda_{em,max}$ = 352 nm and 343 nm, respectively, which is ascribed to the tryptophans in the albumin, *i.e.* in HSA a tryptophan is located at position 214 and in BSA two tryptophan residues exist at positions 134 and 212.

The quenching of the corresponding fluorescence emission band of the SAs which was induced by the presence of the complexes **1–4** was low-to-moderate in the case of HSA (the quenching of the initial HSA fluorescence emission (ΔI/Io) was up to ~43% in the presence of complex **1**, Fig. 5(A)). For BSA, this quenching was moderate-to-significant and more enhanced than HSA (the quenching of the initial BSA fluorescence emission (ΔI/Io) was up to ~66% in the presence of complex **1**, Fig. 5(B)). The observed quenching may be assigned to changes occurring around the tryptophan(s) of SA which are due to changes in albumin secondary structure probably resulting from the binding of the compounds to SAs.

The values of k_q of the complexes were calculated from the Stern-Volmer plots (Figs. S2 and S3) and the Stern-Volmer quenching equation (Eqs. S2 and S3), where $\tau_o = 10^{-8}$ s is the fluorescence lifetime of tryptophan in SA. The obtained k_q values (Table 5) are significantly higher than the value of $10^{10}\,M^{-1}\,s^{-1}$, and may indicate the existence of a static quenching mechanism as a result of the interaction between the compounds and the SAs. Complex **1** shows the highest k_q constants

Table 4
% DPPH scavenging ability (RA%), % ABTS radical scavenging activity (ABTS%), competition % with DMSO for hydroxyl radical (·OH%) for Hoxa and its Zn complexes **1–4**.

Compound	RA%, 20 min	RA%, 60 min	·OH%	ABTS%
Oxaprozin	54.69 ± 0.72	56.86 ± 0.59	64.68 ± 0.41	58.34 ± 0.36
[Zn(oxa)$_2$(MeOH)$_4$], **1**	66.79 ± 0.58	70.95 ± 0.65	81.12 ± 0.38	71.83 ± 0.26
[Zn(oxa)$_2$(H$_2$O)(bipy)], **2**	72.91 ± 0.44	74.62 ± 0.74	88.84 ± 0.36	70.83 ± 0.22
[Zn(oxa)$_2$(bipyam)], **3**	71.52 ± 0.48	72.35 ± 0.14	75.75 ± 0.40	74.92 ± 0.72
[Zn(oxa)$_2$(phen)], **4**	56.67 ± 0.26	68.24 ± 0.31	80.62 ± 0.29	62.44 ± 0.54
NDGA	81.02 ± 0.18	82.60 ± 0.17	Not tested	Not tested
BHT	31.30 ± 0.10	60.00 ± 0.38	Not tested	Not tested
Trolox	Not tested	Not tested	82.80 ± 0.13	91.80 ± 0.17

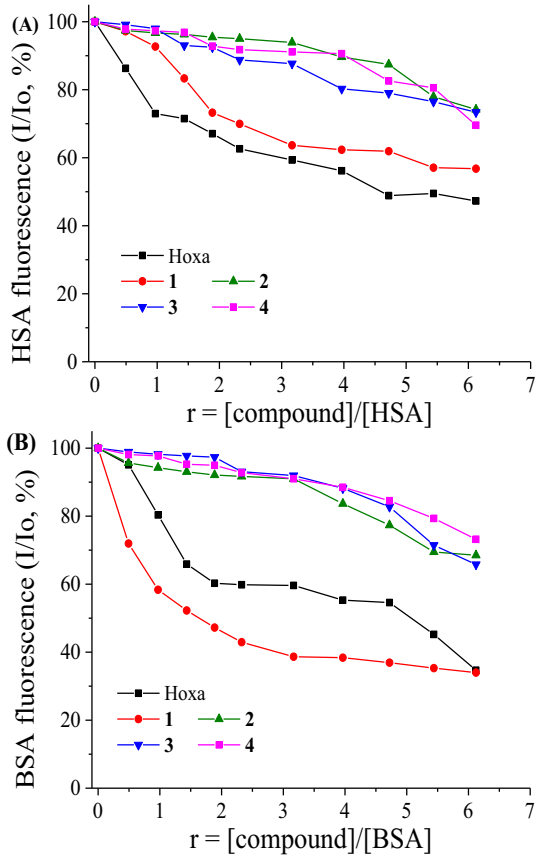

Fig. 5. (A) Plot of relative HSA fluorescence intensity at λ_{em} = 352 nm (I/Io, %) *versus* r (r = [complex] / [HSA]) for complexes **1–4**. (B) Plot of relative BSA fluorescence intensity at λ_{em} = 343 nm (I/Io, %) *versus* r (r = [complex] / [BSA]) for complexes **1–4**.

for both albumins among the herein reported compounds. The k_q constants for complexes **1–4** are within the range found for a series of metal-complexes bearing other NSAIDs as ligands [7,10,14,19,21,23,39–41,50–53].

The values of K for complexes **1–4** were determined from the Scatchard plots (Figs. S4 and S5) and the Scatchard equation (Eq. S4) [54]. The values of K constants of complexes **1–4** (Table 5) are moderate-to-high ($1.13 \times 10^4 - 4.29 \times 10^5\ M^{-1}$) and are similar with those previously reported for metal-NSAID complexes [7,10,14,19,21,23,39–41,50–53]. The SA-binding constants are high enough to show the potency of the complexes to bind to SAs in order to get transported towards their biotargets. On the other hand, the K constants are not too high; indeed, they are significantly lower than the value of $10^{15}\ M^{-1}$ which is the binding constant of diverse compounds with avidin [56] and is among the strongest known non-covalent reversible interactions [57]. Such comparison may serve as proof of a reversible binding between complexes **1–4** and the albumins so that the complexes are transferred to their biological target where they may get released upon arrival.

3.6. Interaction of the compounds with calf-thymus DNA

The interaction of CT DNA with complexes **1–4** was monitored: (a) directly by UV–vis spectroscopy and DNA-viscosity measurements, and (b) indirectly by the ability of the complexes to displace EB from the EB-DNA conjugate which was studied by fluorescence emission spectroscopy.

3.6.1. UV–vis spectroscopic studies

UV–vis spectroscopic titrations are used as first means to evaluate the interaction between DNA and the complexes, so that we may get information relevant to the binding mode and strength of the interaction. The UV–vis spectra of a CT DNA solution were recorded in the presence of increasing concentration of complexes **1–4** and *vice versa*, *i.e.* the UV–vis spectra of the complexes were recorded upon addition of increasing amounts of a CT DNA solution. During such UV–vis spectroscopic titration studies, the existence of any interaction may be concluded when changes of the CT DNA-band at 258–260 nm or the intraligand transition bands of the complexes, respectively, occur, and useful information of this interaction may be initially arisen.

The UV–vis spectra of a CT DNA buffer solution upon addition of increasing concentration of complex **1** are shown representatively in Fig. 6(A). The DNA UV-band at λ_{max} = 258 nm presents slight hypochromism accompanied by a red-shift upon addition of the complex. Similar features are observed in the UV–vis spectra of DNA in the presence of complexes **2–4** and may indicate the existence of an interaction of CT DNA with the complex; such interaction may result in the formation of a new conjugate between DNA and the complex under study which seems to stabilize the CT DNA double-helix [58].

In the UV–vis spectra of complex **2** (Fig. 6(B)) as well as complexes **1**, **3** and **4** (Table 6), the intra-ligand band with λ_{max} = 279 nm exhibited a slight hyperchromism upon addition of CT DNA. The observed changes in the UV–vis spectra of the complexes in the presence of CT DNA cannot lead to a final conclusion regarding the interaction mode and, in order to further investigate this interaction, it is necessary to perform more experiments such as DNA-viscosity measurements.

The values of K_b of complexes **1–4** were calculated *via* plots [DNA]/(ε_A-ε_f) *versus* [DNA] (Fig. S6) and the Wolfe-Shimer equation (Eq. S5) [59]. The K_b constants of complexes **1–4** (Table 6) may reveal the strong binding of the complexes to CT DNA. Complex **3** presents the highest K_b constant ($= 2.47(\pm 0.31) \times 10^6\ M^{-1}$) among the complexes. The complexes have similar K_b values with the reported Zn complexes with the NSAIDs diflunisal [7], flufenamic acid [14], mefenamic acid [19], niflumic acid [21], and tolfenamic acid [23].

3.6.2. DNA-viscosity studies

The interaction of the compounds with CT DNA was also investigated *via* measurements of the viscosity of a DNA solution in the presence of the compounds. As known, the relative viscosity of a DNA solution (η/η_0) is sensitive to the relative DNA-length changes (L/L_0) which may occur in the presence a DNA-binder and they are correlated *via* the equation $L/L_0 = (\eta/\eta_0)^{1/3}$ [58]. In the case of intercalation, the relative DNA-viscosity will show an increase, while it will decrease slightly or remain unchanged in the case of nonclassical intercalation, *i.e.* groove-binding or electrostatic interaction [58].

In the presence of increasing concentration of the compounds (up to

Table 5
The albumin (HSA/BSA)-quenching (k_q) and binding (K) constants for Hoxa and its Zn complexes **1–4**.

Compound	$k_{q(HSA)}$ ($M^{-1}\,s^{-1}$)	$K_{(HSA)}$ (M^{-1})	$k_{q(BSA)}$ ($M^{-1}\,s^{-1}$)	$K_{(BSA)}$ (M^{-1})
Oxaprozin	$5.80(\pm 0.30) \times 10^{12}$	$1.65(\pm 0.05) \times 10^5$	$7.13(\pm 0.32) \times 10^{12}$	$1.06(\pm 0.06) \times 10^5$
$[Zn(oxa)_2(MeOH)_4]$, **1**	$5.84(\pm 0.31) \times 10^{12}$	$1.42(\pm 0.04) \times 10^5$	$1.71(\pm 0.10) \times 10^{13}$	$4.13(\pm 0.10) \times 10^5$
$[Zn(oxa)_2(H_2O)(bipy)]$, **2**	$1.81(\pm 0.05) \times 10^{12}$	$9.74(\pm 0.74) \times 10^4$	$1.67(\pm 0.10) \times 10^{13}$	$4.29(\pm 0.10) \times 10^5$
$[Zn(oxa)_2(bipyam)]$, **3**	$1.97(\pm 0.05) \times 10^{12}$	$1.13(\pm 0.07) \times 10^4$	$5.00(\pm 0.30) \times 10^{11}$	$1.85(\pm 0.30) \times 10^5$
$[Zn(oxa)_2(phen)]$, **4**	$1.52(\pm 0.05) \times 10^{12}$	$1.31(\pm 0.11) \times 10^4$	$1.07(\pm 0.03) \times 10^{12}$	$4.60(\pm 0.30) \times 10^4$

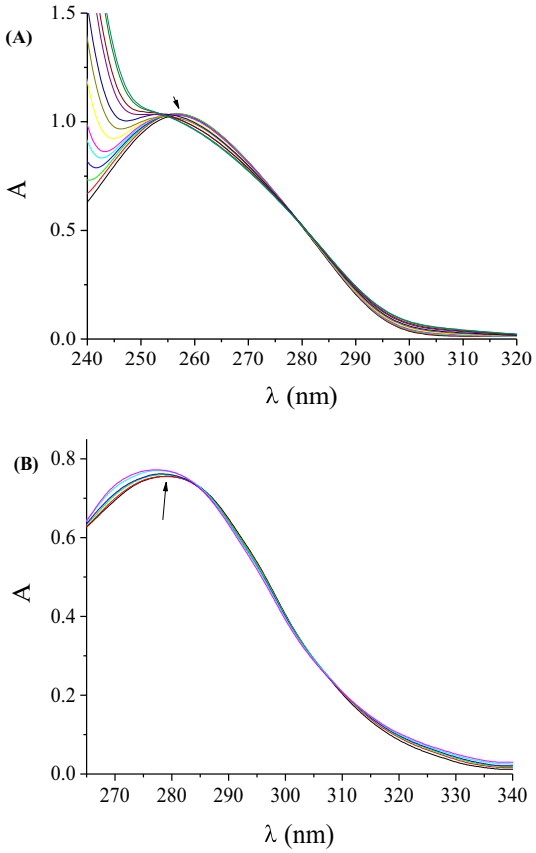

Fig. 6. (A) UV–vis spectra of CT DNA (0.15 mM) in buffer solution (150 mM NaCl and 15 mM trisodium citrate at pH 7.0) in the absence or presence of complex **1**. The arrow shows the changes upon increasing amounts of the complex. (B) UV–vis spectra of DMSO solution of complex **2** (10 μM) in the presence of increasing amounts of CT DNA.

Table 6
UV–vis spectral features of the interaction of complexes **1–4** with CT DNA. UV-band (λ in nm) (percentage of the observed hyper-/hypo-chromism ($\Delta A/A_o$, %), blue-/red-shift of the λ_{max} ($\Delta\lambda$, nm)) and DNA-binding constants (K_b).

Compound	λ (nm) ($\Delta A/A_o$[a], $\Delta\lambda$[b])	K_b (M^{-1})
Oxaprozin	291 (−1.3, +0.6)	1.00(± 0.14) × 10^6
$[Zn(oxa)_2(MeOH)_4]$, **1**	275 (+7.6, −1)	4.89(± 0.72) × 10^5
$[Zn(oxa)_2(H_2O)(bipy)]$, **2**	279 (+1.4, −2)	8.83(± 1.28) × 10^4
$[Zn(oxa)_2(bipyam)]$, **3**	272 (+6.7, −1)	2.47(± 0.31) × 10^6
$[Zn(oxa)_2(phen)]$, **4**	267 (+10.5, −1)	1.84(± 0.26) × 10^4

[a] "+" denotes hyperchromism, "-" denotes hypochromism.
[b] "+" denotes red-shift, "-" denotes blue-shift.

the value of $r = 0.35$, Fig. 7), the relative viscosity of a CT DNA solution (0.1 mM) showed an increase. Such behavior may be due to the existence of intercalation of the compounds to the DNA. This intercalation may obviously take place through the insertion of the complexes in-between the DNA-bases and will result in an increase of the separation distances among the DNA bases in order to accommodate the intercalating compounds; therefore, the relative DNA-viscosity shows an increase. This conclusion of intercalation comes to shed light on the findings during the UV–vis spectroscopic studies.

3.6.3. EB-competition studies

EB intercalates to DNA when the planar EB-phenanthridine ring inserts in-between DNA-bases forming an EB-DNA conjugate; the solution containing this conjugate exhibits an intense fluorescence emission band at 592 nm, when it is excited at 540 nm. A compound which

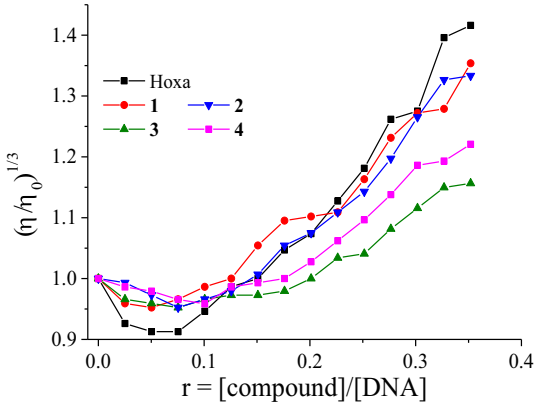

Fig. 7. Relative viscosity $(\eta/\eta_o)^{1/3}$ of CT DNA (0.1 mM) in buffer solution (150 mM NaCl and 15 mM trisodium citrate at pH 7.0) in the presence of complexes **1–4** at increasing amounts (r = [complex] / [DNA]).

acts as a DNA-intercalator, when bound to DNA equally to or more tightly than EB, may displace EB from the EB-DNA conjugate; this displacement will induce a noteworthy quenching of the EB-DNA fluorescence emission band [54,60]. The fluorescence emission spectra of the EB-DNA conjugate were recorded in the presence of increasing amounts of complexes **1–4** (representatively shown for **2** in Fig. 8). The moderate-to-significant quenching (arising up to 72% of the initial EB-DNA fluorescence) induced by the presence of the compounds (Fig. S7, Table 7) may suggest that the complexes can displace EB from EB-DNA conjugate as a consequence of the competition for the DNA-intercalating sites; thus, the intercalation of the compounds to CT DNA can be indirectly suggested.

According to the Stern-Volmer plots (Fig. S8), the observed quenching of the EB-DNA fluorescence has been found to be in good agreement ($R = 0.99$) with the linear Stern-Volmer equation (Eq. S2) [61]. The calculated K_{SV} constants of the complexes (Table 7) are in the range reported for other metal-NSAIDs complexes [7,10,14,19,21,23,39–41,50–53], with complex **3** showing the highest K_{SV} constant among the Zn-oxaprozin complexes. A comparison of the K_{SV} constants of complexes **1–4** with other Zn-NSAIDs complexes may reveal that complexes **1–4** have similar or slightly higher K_{SV} values than the corresponding zinc complexes with the NSAIDs diflunisal [7], mefenamic acid [19], niflumic acid [21], tolfenamic acid [23] and flufenamic acid [14]. The k_q constants (Table 7) are significantly higher than the value of $10^{10}\ M^{-1}\ s^{-1}$ suggesting that the quenching of the EB-

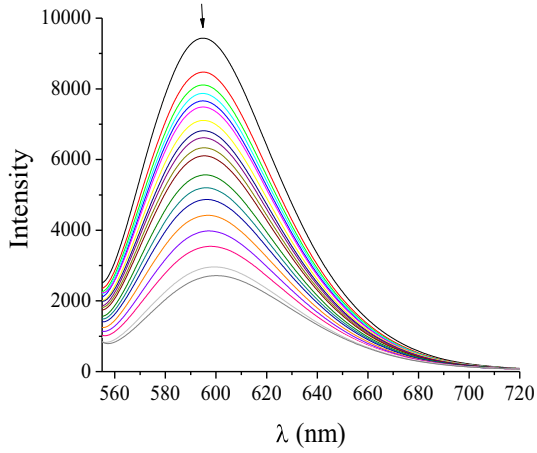

Fig. 8. Fluorescence emission spectra (λ_{exc} = 540 nm) for EB-DNA ([EB] = 20 μM, [DNA] = 30 μM) in buffer solution in the absence and presence of increasing amounts of complex **2**. The arrow shows the changes of intensity upon increasing amounts of **2**.

Table 7
Percentage of EB-DNA fluorescence quenching (ΔI/Io, %), Stern-Volmer constants (K_{SV}) and quenching constants of the EB-DNA fluorescence (k_q) for complexes **1–4**.

Compound	ΔI/Io (%)	K_{sv} (M^{-1})	k_q ($M^{-1}\,s^{-1}$)
Oxaprozin	70	$1.42(\pm 0.06)\times 10^5$	$6.18(\pm 0.25)\times 10^{12}$
$[Zn(oxa)_2(MeOH)_4]$, **1**	71	$9.81(\pm 0.27)\times 10^5$	$4.27(\pm 0.12)\times 10^{13}$
$[Zn(oxa)_2(H_2O)(bipy)]$, **2**	72	$7.43(\pm 0.20)\times 10^5$	$3.23(\pm 0.09)\times 10^{13}$
$[Zn(oxa)_2(bipyam)]$, **3**	72	$1.17(\pm 0.04)\times 10^6$	$5.08(\pm 0.19)\times 10^{13}$
$[Zn(oxa)_2(phen)]$, **4**	72	$3.34(\pm 0.10)\times 10^5$	$1.45(\pm 0.04)\times 10^{13}$

DNA fluorescence from the complexes takes place *via* a static mechanism [62], which further verifies the displacement of EB from EB-DNA conjugate.

4. Conclusions

Four novel zinc(II) complexes with the NSAID oxaprozin as ligand and the *N,N′*-donors 2,2′-bipyridylamine, 1,10-phenanthroline or 2,2′-bipyridine as co-ligands have been successfully prepared and thoroughly characterized. The crystal structures of complexes **2–4** were determined by single-crystal X-ray crystallography. In the complexes, the deprotonated oxaprozin ligands are bound to zinc(II) ion in a monodentate and/or a bidentate fashion.

The potential *in vitro* bioactivity of the resultant complexes was evaluated in regard to their ability to scavenge free radicals such as DPPH, ABTS and hydroxyl, their ability to bind to CT DNA and their affinity to albumins BSA and HSA. Concerning their behavior towards the free radicals, the complexes showed higher scavenging activity than free oxaprozin and they are very active scavengers of hydroxyl radicals.

The interaction of the complexes with both albumins revealed their potency to get bound tightly and reversibly to them in order to get transferred safely towards their potential biotargets and possibly get released upon their arrival.

As for the interaction of the complexes with CT DNA, intercalation is considered as the most probable mode of interaction between the complexes and DNA as revealed by the techniques used. Complexes **1–4** seem to be better DNA-binders than free oxaprozin, with complex $[Zn(oxa)_2(bipyam)]$, **3** having the highest DNA-binding constant ($K_b = 2.47(\pm 0.31)\times 10^6\,M^{-1}$) among the compounds under study.

The existing results concerning the bioactivity of Zn-oxaprozin complexes **1–4** may be considered promising for more advanced biological studies and potential applications.

Abbreviations

ABTS	2,2′-azinobis(3-ethylbenzothiazoline-6-sulfonic acid) radical cation
BHT	butylated hydroxytoluene
bipy	2,2′-bipyridine
bipyam	2,2′-bipyridylamine
BSA	bovine serum albumin
CT	calf-thymus
DMSO	dimethylsulfoxide
DPPH	1,1-diphenyl-picrylhydrazyl
EB	ethidium bromide, 3,8-diamino-5-ethyl-6-phenyl-phenanthridinium bromide
Hoxa	oxaprozin
HSA	human serum albumin
K	SA-binding constant
K_b	DNA-binding constant
k_q	quenching constant
K_{SV}	Stern-Volmer constant
m	medium
NDGA	nordihydroguaiaretic acid
NSAID	non-steroidal anti-inflammatory drug
phen	1,10-phenanthroline
r	[compound]/[DNA] ratio
RA%	DPPH scavenging activity
s	strong
SA	serum albumin
sh	shoulder
trolox	6-hydroxy-2,5,7,8-tetramethylchromane-2-carboxylic acid
vs	very strong
$\Delta\nu(CO_2)$	$\nu_{asym}(CO_2)-\nu_{sym}(CO_2)$

Appendix A. Supplementary data

CCDC 1896361-1896363 contain the supplementary crystallographic data for compounds **2–4**. These data can be obtained free of charge *via* www.ccdc.cam.ac.uk/conts/retrieving.html (or from the Cambridge Crystallographic Data Centre, 12 Union Road, Cambridge CB21EZ, UK; fax: (+44) 1223-336-033; or deposit@ccde.cam.ac.uk).Supplementary data associated with this article can be found, in the online version, at doi: https://doi.org/10.1016/j.jinorgbio.2019.03.016.

References

[1] G.K. Walkup, S.C. Burdette, S.J. Lippard, R.Y. Tsien, J. Am. Chem. Soc. 122 (2000) 5644–5645.
[2] B.L. Vallee, D.S. Auld, Biochemistry 32 (1993) 6493–6500.
[3] C.P. Larson, U.R. Saha, H. Nazrul, PLoS Med. 6 (2009) e1000175.
[4] H. Sakurai, Y. Kojima, Y. Yoshikawa, K. Kawabe, H. Yasui, Coord. Chem. Rev. 226 (2002) 187–198.
[5] Q. Zhou, T.W. Hambley, B.J. Kennedy, P.A. Lay, P. Turner, B. Warwick, J.R. Biffin, H.L. Regtop, Inorg. Chem. 39 (2000) 3742–3748.
[6] A. Tarushi, K. Lafazanis, J. Klun, I. Turel, A.A. Pantazaki, G. Psomas, D.P. Kessissoglou, J. Inorg. Biochem. 121 (2013) 53–65.
[7] A. Tarushi, C. Kakoulidou, C.P. Raptopoulou, V. Psycharis, D.P. Kessissoglou, I. Zoi, A.N. Papadopoulos, G. Psomas, J. Inorg. Biochem. 170 (2017) 85–97.
[8] J.S. Casas, E.E. Castellano, M.D. Couce, J. Ellena, A. Sanchez, J. Sordo, C. Taboada, J. Inorg. Biochem. 100 (2006) 124–132.
[9] M. Di Vaira, C. Bazzicalupi, P. Orioli, L. Messori, B. Bruni, P. Zatta, Inorg. Chem. 43 (2004) 3795–3797.
[10] G. Psomas, D.P. Kessissoglou, Dalton Trans. 42 (2013) 6252–6276.
[11] P. Lemoine, B. Viossat, N.H. Dung, A. Tomas, G. Morgant, F.T. Greenaway, J.R.J. Sorenson, J. Inorg. Biochem. 98 (2004) 1734–1749.
[12] H.A. Ali, B. Jabali, Polyhedron 107 (2016) 97–106.
[13] A. Tarushi, F. Kastanias, V. Psycharis, C.P. Raptopoulou, G. Psomas, D.P. Kessissoglou, Inorg. Chem. 51 (2012) 7460–7462.
[14] A. Tarushi, P. Kastanias, C.P. Raptopoulou, V. Psycharis, D.P. Kessissoglou, A.N. Papadopoulos, G. Psomas, J. Inorg. Biochem. 163 (2016) 332–345.
[15] R. Smolkova, V. Zelenak, L. Smolko, D. Sabolova, J. Kuchar, R. Gyepes, J. Inorg. Biochem. 177 (2017) 143–158.
[16] H.A. Ali, S.N. Omar, M.D. Darawsheh, H. Fares, J. Coord. Chem. 69 (2016) 1110–1122.
[17] N.C. Kasuga, K. Sekino, M. Ishikawa, A. Honda, M. Yokoyama, S. Nakano, N. Shimada, C. Koumo, K. Nomiya, J. Inorg. Biochem. 96 (2003) 298–310.
[18] B. Jabali, H.A. Ali, Polyhedron 117 (2016) 249–258.
[19] A. Tarushi, Z. Karaflou, J. Kljun, I. Turel, G. Psomas, A.N. Papadopoulos, D.P. Kessissoglou, J. Inorg. Biochem. 128 (2013) 85–96.
[20] A.A. Khandar, Z. Mirzaei-Kalar, J. White, S.A. Hosseini-Yazdi, A. Jouyban, J. Mol. Liq. 224 (2016) 684–693.
[21] A. Tarushi, C.P. Raptopoulou, V. Psycharis, D.P. Kessissoglou, A.N. Papadopoulos, G. Psomas, J. Inorg. Biochem. 176 (2017) 100–112.
[22] R. Smolkova, V. Zelenak, L. Smolko, J. Kuchar, M. Rabajdova, M. Ferencakova, M. Marekova, Eur. J. Med. Chem. 153 (2018) 131–139.
[23] A. Tarushi, X. Totta, A. Papadopoulos, J. Kljun, I. Turel, D.P. Kessissoglou, G. Psomas, Eur. J. Med. Chem. 74 (2014) 187–198.
[24] A. Tarushi, X. Totta, C. Raptopoulou, V. Psycharis, G. Psomas, D.P. Kessissoglou, Dalton Trans. 41 (2012) 7082–7091.
[25] Oxaprozin in Meyler's Side Effects of Drugs, 2006, 15th ed., 2643–2644.
[26] R. Jamar, J. Dequeker, Curr. Med. Res. Opin. 5 (1978) 433–438.
[27] D.J. Greenblatt, R. Matlis, J.M. Scavone, G.T. Blyden, J.S. Harmatz, R.I. Shader, Brit. J. Clin. Pharmacol. 19 (1985) 373–378.
[28] S. Dutta, S. Padhye, V. Mckee, Inorg. Chem. Commun. 7 (2004) 1071–1074.
[29] M.F. Reichmann, S.A. Rice, C.A. Thomas, P. Doty, J. Am. Chem. Soc. 76 (1954) 3047–3053.
[30] J. Marmur, J. Mol. Biol. 3 (1961) 208–211.
[31] Bruker Analytical X-ray Systems, Inc. Apex2, Version 2 User Manual, M86-E01078, Madison, WI, (2006).

[32] Siemens Industrial Automation, Inc. SADABS: Area-Detector Absorption Correction; Madison, WI, (1996).
[33] L. Palatinus, G. Chapuis, J. Appl. Crystallogr. 40 (2007) 786–790.
[34] P.W. Betteridge, J.R. Carruthers, R.I. Cooper, K. Prout, D.J. Watkin, J. Appl. Crystallogr. 36 (2003) 1487.
[35] D.J. Watkin, C.K. Prout, L.J. Pearce, CAMERON Program, Oxford University, UK, Chemical Crystallographic Laboratory, 1996.
[36] W.J. Geary, Coord. Chem. Rev. 7 (1971) 81–122.
[37] K. Nakamoto, Infrared and Raman Spectra of Inorganic and Coordination Compounds, Part B: Applications in Coordination, Organometallic, and Bioinorganic Chemistry, sixth ed., Wiley, New Jersey, 2009.
[38] A.W. Addison, T.N. Rao, J. Reedijk, J. van Rijn, G.C. Verschoor, J. Chem. Soc., Dalton Trans. (1984) 1349–1356.
[39] M. Zampakou, N. Rizeq, V. Tangoulis, A.N. Papadopoulos, F. Perdih, I. Turel, G. Psomas, Inorg. Chem. 53 (2014) 2040–2052.
[40] X. Totta, A.G. Hatzidimitriou, A.N. Papadopoulos, G. Psomas, New J. Chem. 41 (2017) 4478–4492.
[41] F. Dimiza, C.P. Raptopoulou, V. Psycharis, A.N. Papadopoulos, G. Psomas, New J. Chem. 42 (2018) 16666–16681.
[42] L.P. Battaglia, A. Bonamartini-Corradi, G. Marcotrigiano, L. Menabue, G.C. Pellacani, Inorg. Chem. 18 (1979) 148–152.
[43] L. Yang, D.R. Powell, R.P. Houser, Dalton Trans. (2007) 955–964.
[44] A. Okuniewski, D. Rosiak, J. Chojnacki, B. Becker, Polyhedron 90 (2015) 47–57.
[45] R. Cini, G. Giorgi, A. Cinquantini, C. Rossi, M. Sabat, Inorg. Chem. 29 (1990) 5197–5200.
[46] S. Dairi, M. Carbonneau, T. Galeano-Diaz, H. Remini, F. Dahmoune, O. Aoun, A. Belbahi, C. Lauret, J. Cristol, K. Madani, Food Chem. 237 (2017) 297–304.
[47] A. Slavova-Kazakova, M. Karamac, V. Kancheva, R. Amarowicz, Molecules 21 (2016) 17.
[48] C. Kontogiorgis, M. Ntella, L. Mpompou, F. Karallaki, A. Papadopoulos, D. Hadjipavlou-Litina, D. Lazari, J. Enzyme Inhib, Med. Chem. 31 (2016) 154–159.
[49] C. Kontogiorgis, D. Hadjipavlou-Litina, J. Enzyme Inhib, Med. Chem. 18 (2003) 63–69.
[50] S. Perontsis, A.G. Hatzidimitriou, A.N. Papadopoulos, G. Psomas, J. Inorg. Biochem. 162 (2016) 9–21.
[51] M. Zampakou, A.G. Hatzidimitriou, A.N. Papadopoulos, G. Psomas, J. Coord. Chem. 68 (2015) 4355–4372.
[52] X. Totta, A.A. Papadopoulou, A.G. Hatzidimitriou, A. Papadopoulos, G. Psomas, J. Inorg. Biochem. 145 (2015) 79–93.
[53] A. Tarushi, C.P. Raptopoulou, V. Psycharis, D.P. Kessissoglou, A.N. Papadopoulos, G. Psomas, J. Inorg. Biochem. 140 (2014) 185–198.
[54] J.R. Lakowicz, Principles of Fluorescence Spectroscopy, third ed., Plenum Press, New York, 2006.
[55] C. Tan, J. Liu, H. Li, W. Zheng, S. Shi, L. Chen, L. Ji, J. Inorg. Biochem. 102 (2008) 347–358.
[56] O.H. Laitinen, V.P. Hytonen, H.R. Nordlund, M.S. Kulomaa, Cell. Mol. Life Sci. 63 (2006) 2992–3017.
[57] V. Rajendiran, R. Karthik, M. Palaniandavar, H. Stoeckli-Evans, V.S. Periasamy, M.A. Akbarsha, B.S. Srinag, H. Krishnamurthy, Inorg. Chem. 46 (2007) 8208–8221.
[58] J.L. Garcia-Gimenez, M. Gonzalez-Alvarez, M. Liu-Gonzalez, B. Macias, J. Borras, G. Alzuet, J. Inorg. Biochem. 103 (2009) 923–934.
[59] A. Wolfe, G. Shimer, T. Meehan, Biochemistry 26 (1987) 6392–6396.
[60] W.D. Wilson, L. Ratmeyer, M. Zhao, L. Strekowski, D. Boykin, Biochemistry 32 (1993) 4098–4104.
[61] G. Zhao, H. Lin, S. Zhu, H. Sun, Y. Chen, J. Inorg. Biochem. 70 (1998) 219–226.
[62] D.P. Heller, C.L. Greenstock, Biophys. Chem. 50 (1994) 305–312.